Macromolecules
ARTICLE

Macromolecules **2009**, *42*, 8241–8250 **8241**
DOI: 10.1021/ma901780e

Structure and Mobility of Poly(ethylene terephthalate): A Molecular Dynamics Simulation Study

Hossein Eslami*,†,‡ and Florian Müller-Plathe†

†*Eduard-Zintl Institut für Anorganische und Physikalische Chemie, Technische Universität Darmstadt, Petersenstrasse 20, D-64287, Germany, and* ‡*Department of Chemistry, College of Sciences, Persian Gulf University, Boushehr 75168, Iran*

Received August 8, 2009; Revised Manuscript Received September 4, 2009

ABSTRACT: An accurate force-field has been parametrized for PET and is employed to simulate a long chain, consisting of 120 repeat units, over a wide temperature and pressure range, for long time scales. The force field has been validated against the experimental results for the pressure−volume−temperature properties, the characteristic ratio, the dipolar ratio, and the population of ethylene glycol bond conformer. In all cases the agreement with experiment is quite good. The glass transition temperature is calculated very accurately as a function of pressure. The local dynamics of the chain has been investigated by calculating phenylene reorientation, collective dipole moment, and individual dipole moment correlation functions. The calculated relaxation times for collective dipole moment and phenylene reorientation correlation functions show activation energies close to the corresponding experimental β-relaxation value. Local translational mobilities of phenylene groups in the backbone and end phenylene groups have also been investigated. It is concluded that the end groups have much higher mobility than the polymer backbone, and increasing the distance from the chain ends decreases the mobility dramatically. The long-time asymptotic slope of chain displacement at temperatures higher than the glass transition temperature is around 0.65 in close agreement with Rouse model. On the other hand at the glassy state, the polymer segments perform very restricted movements in the cages formed by their surrounding segments.

Introduction

Poly(ethylene terephthalate) (PET) is the most important polyester, used for many applications such as food packaging for ovenable food trays and beverage packaging, due to its superior barrier properties in comparison with polyolefins, polycarbonates, polystyrene, and other polymers.[1,2] PET is also being used in textile fibers, films, and molded products.[1,2] Reinforced short fibers of PET are applied in the manufacture of windshield wiper arms, brake systems, motor end frames, microswitches, coil forms, lamp sockets, oven handles, iron skirts, etc.[2,3] In fact, among all plastics, PET is of particular attention in terms of possibility of recycling of PET bottles.[4]

PET can be easily prepared over a range of crystallinities, ranging from 0% to 50%, depending on the thermal treatment rate. Even by quenching PET from the melt into liquid nitrogen, Schmidt-Rohr et al.[5] found a residual crystallinity of around 5%. They concluded that the relatively low crystallization rate of PET is mainly due to the low-trans probability of the melt. Experimental measurements, such as dynamic mechanical experiments,[6] dielectric spectroscopy,[7−9] thermally stimulated depolarization currents,[10] and differential scanning calorimetry,[11] have revealed the existence of two distinct amorphous phases in PET. Because of the fact that PET can be obtained either in the amorphous state or with a controlled amount of crystallinity, it has been frequently addressed as an example of a semicrystalline polymer. As a result, many experimental studies of the effect of crystallinity on a variety of physical properties including mechanical and dielectric relaxational behavior,[6−9,12] thermal behavior,[13−15] and structure development,[16−18] have been performed on PET.

Although PET has been studied widely from the experimental point of view, there is still much to be learned about the connection of its bulk properties to molecular properties. Computer simulation methods are very efficient in obtaining insights into the molecular origins of the behavior of bulk polymers. Despite considerable experimental research on PET, computer simulation studies of this polymer are relatively rare. This is because of the fact that PET has a complex chemical structure, which forbids the use of advanced Monte Carlo methods, and the glassy polymer has a long relaxation time, which makes the MD simulation studies of this polymer difficult.

Early Monte Carlo (MC) simulation studies of PET goes back to the work of Tanaka et al.[19] on the study of molecular structure by dielectric measurements and MC calculations. In a similar study, conformational analysis of models of dimers and pentamers of PET was performed by Auriemma et al.,[20] using the MC technique. MC chain generation techniques, based on the rotational isometric states (RIS) model, were also used by Taylor et al.,[21] by Cail et al.,[22] and by Chen and Zhang[23] to study conformational and orientational properties of PET. In a recent study by Kamio et al.,[24] the end bridging MC has been applied to study coarse-grained PET chains.

Molecular dynamics (MD) simulation studies of PET include the work of Hedenqvist et al.,[25] in which they developed a united atom model of PET to obtain structure and relaxation in amorphous PET. In a subsequent article, Boyd and Boyd[26] applied the same united atom model, but modified their original torsional potentials to reflect the results of quantum chemistry calculations and to accommodate more precise experimental

*Corresponding author. E-mail: h.eslami@theo.chemie.tu-darmstadt.de.

Published on Web 09/17/2009

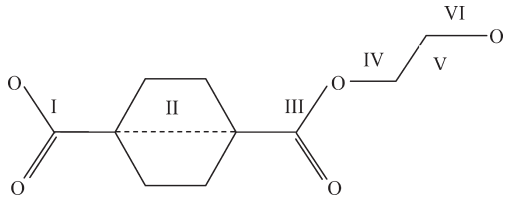

Figure 1. PET repeat-unit RIS bond assignments. The bond types are indicated by Greek numbers.

knowledge of the gauche/trans ratio of the ethylene glycol bond. In both studies,[25,26] the calculated densities of PET in the glassy state are not in good agreement with experimental data.[12,27,28] In the former study the density of PET melts is in a good agreement with experiment,[27] but the glass transition temperature deviates more than 100 K from experiment. Although in the later study, the improved force-field by Boyd and Boyd,[26] improved the accuracy of calculations, still they have obtained a glass transition temperature which deviates more than 50 K from experimental value. Moreover, in this case their calculated densities of PET melt are less accurate then those of the former study. Other molecular dynamics simulation studies of PET consist of the reports by Bharadwaj and Boyd[29] and by Shanks and Pavel[30] on the diffusion and sorption of gases in PET, and that of Pavel and Shanks[31] on the diffusion coefficient of small molecules in blends of bulk amorphous PET and related alkylen and aromatic polyesters.

In a recent study by Karayiannis et al.[32] detailed atomistic simulations concerning the structural, conformational, dynamic, and diffusion coefficients of oxygen and carbon dioxide in PET have been reported. They chose a single chain of PET of 80 repeating units and created equilibrium structures according to a method proposed by Hofmann et al.,[33,34] in which an equilibration cycle consisting of a series of relatively short *NPT* and *NVT* MD simulations is applied. While this method is fast, it has, however, two major drawbacks: (1) only one equilibrated glassy polymer structure is generated at the end of the cycle, and (2) the finally generated configuration may not be in equilibrium as a result of short MD simulation stages. Karayiannis et al.[32] extended the equilibration cycle of Hofmann et al.[33,34] and generated equilibrium PET samples at 600 K by changing the pressure to force the model density to match the experimental value. Their calculations show that the diffusivity of gases in PET strongly depends on the predicted density of PET. Therefore, they could obtain a diffusivity close to the experimental one at states where the density was forced to match the experimental density.

This work aims to perform detailed atomistic MD simulation of PET. In particular our simulation is different from previously reported simulations in the following ways: (1) developing an accurate force-field for PET (its accuracy is checked against experimental pressure-volume-temperature data, characteristic ratio, dipolar ratio, and population of ethylene glycol bond conformer); (2) simulating longer chains of PET (120 monomer units) over a wide temperature range, ranging from 280 to 600 K; (3) performing simulations over a broad range of pressures, varying from atmospheric pressures to pressures as high as 200 MPa and studying the pressure effect on the glass transition temperature; (4) performing simulations for much longer time scales (30 ns).

Chain Generation

We open this section with a historical review of the original RIS model and the refined RIS models employed in previous MD simulations, addressed in the preceding section.[25,26] The polymer conformations are described, in terms of a Markov model of torsional state probabilities, by the RIS model originally developed by Williams and Flory.[35] In the RIS model of PET, each repeat unit is divided into six specific backbone torsions, as it is indicated in Figure 1. Bond II is a virtual bond which spans the terephthaloyl unit. Polymer must adopt either a *cis* or a *trans* conformation with respect to this bond, in order to have coplanar conformations of the aromatic ring and the ester groups. An independent statistical weight, σ_i, pertaining to all rotational states of bond i can be expressed in the form of statistical weight matrices. According to William and Flory's[35] model of PET, the carbonyl groups are restricted to the *trans* conformation, and hence the statistical weights $\sigma_I = \sigma_{III} = 1$ for the ith bond in the *trans* state, irrespective of the conformation of the previous bonds. On the basis of the comparison between the calculated dipole moments of dimethyl and diethyl terephthalate with experiment, the statistical weight σ_{II} was also assumed by Williams and Flory[35] to be unity. Finally, to be able to predict the correct characteristic ratio compared to the assumed experimental value,[36,37] the statistical weight parameters associated with bonds IV, V, and VI were assumed by Williams and Flory[35] to be 0.5, 1.5, and 0.5, respectively, when the ith bond is in the *gauche* state versus unity in the *trans* state. Moreover, the five-center interactions, ω, were assigned, at bond pairs IV−V and V−VI, as 0.1.

Following the afore-cited assumptions, Williams and Flory[35] calculated the mean-square end-to-end distances in PET chains up to 100 repeating units. The characteristic ratio can be calculated as follows:

$$C_\infty = \frac{\langle R^2 \rangle}{M} \tag{1}$$

Here C_∞ is the average characteristic ratio, R^2 is the square end-to-end distance, M is the chain molecular weight in g mol^{-1}, and the brackets indicate the average. Their calculated average characteristic ratio, 9.3×10^{-3} nm^2 mol g^{-1}, were comparable to the experimental values determined from the results of intrinsic viscosity measurements (10.4 nm^2 mol g^{-1}).[36,37] However, there are some not necessarily consistent reports in the literature on the conformational analysis of PET. In fact, the unperturbed chain dimensions of PET have been indirectly estimated form viscometric data, obtained in some typical good solvents like trifluoroacetic acid. Therefore, the main difficulty stems from very low solubility of PET in typical solvents, and hence, the estimated unperturbed end-to-end distances are considerably scattered.[36−41] At this point it is worth considering that, in the previous MD simulation studies of Hedenqvist et al.,[25] Boyd and Boyd,[26] and Karayiannis et al.,[32] the authors have all calculated a characteristic ratio very close to the reported value by Williams and Flory.[35] However, more recent small-angle neutron scattering experiments, by Gilmer et al.,[42] performed on partially deuterated amorphous PET samples at 523 K, shows a considerably lower characteristic ratio in the range between $(6.1-6.9)\times10^{-3}$ nm^2 mol g^{-1}. More recent calculations by Taylor et al.[21] and by Cail et al.[22] using a RIS model of PET show that adjusting the statistical weight σ_V plays an important role in predicting a characteristic ratio comparable to the reported value by Gilmer et al.[42] Very recently Sasanuma[43] performed conformational analysis of PET by the refined RIS model coupled with *ab initio* molecular orbital calculations for ethylene glycol dibenzoate, as a model compound. The calculated characteristic ratios based on Sasanuma's calculations also ranges from $(6.0-6.5)\times10^{-3}$ nm^2 mol g^{-1} at temperatures ranging from 298 to 523 K.[43] In this work the RIS method of Cail et al.[22] has been applied to generate a PET chain of 120 repeat units in vacuum. The results on the calculated characteristic ratio, dipolar ratio, and population of ethylene glycol bond, which are all related to the conformation of generated chain are given in the following sections.

Table 1. Force Field Parameters for Poly(ethylene terephthalate)[a]

Bond Lengths

bond	length (nm)	bond	length (nm)
H_c-O^b	0.0970	C_a-H_a	0.108
$O-C_c{}^b$	0.1353	$O-C_b$	0.141
C_c-O_c	0.1229	C_b-H_b	0.109
C_c-C_{a1}	0.1409	C_b-C_b	0.1526
C_a-C_a	0.140		

Angle Bendings
$U_{angle} = \frac{1}{2}k_{angle}(\theta_{ijk}-\theta^0_{ijk})^2$

$i-j-k$	θ^0 (deg)	k_{angle} (kJ mol^{-1} rad^{-2})
H_c-O-C_c	113.0	293.0
$O-C_c-O_c$	120.0	669.9
$O_c-C_c-C_{a1}$	120.0	669.9
$O-C_c-C_{a1}$	120.0	586.1
$C_c-C_{a1}-C_a$	120.0	527.5
$C_a-C_a-C_a$	120.0	527.5
C_a-C_a-H_a	120.0	293.0
$C_c-O-C_b{}^b$	112.8	472.8
$O-C_b-H_b$	109.5	418.7
$O-C_b-C_b$	109.5	418.7
$H_b-C_b-H_b$	109.5	293.1
$H_b-C_b-C_b$	109.5	418.7

Harmonic Dihedrals
$U_d = \frac{1}{2}k_d(\varphi_{ijkl}-\varphi^0_{ijkl})^2$

$i-j-k-l$	φ^0 (deg)	k_d (kJ mol^{-1})
$C_c-C_a-C_a-C_a$	180.0	207.5
$C_a-C_a-C_a-C_a$	0.0	207.5
$H_a-C_a-C_a-H_a$	0.0	207.5

Torsions
$U_{tor} = \sum_p \frac{k_{tor}}{2}[1-\cos(p(\varphi_{ijkl}-\varphi^0_{ijkl}))]$

$i-j-k-l$	periodicity	φ^0 (deg)	k_{tor} (kJ mol^{-1})
$H_c-O-C_c-C_{a1}$	1	180	30.0
$O-C_c-C_{a1}-C_a$	2	180	22.0
$O_c-C_c-C_{a1}-C_a$	2	180	22.0
$C_b-O-C_c-C_{a1}$	1	180	30.0
$C_b-C_b-O-C_c$	2	90	3.20
	3	60	7.85
$O-C_b-C_b-O$	1	180	7.80
	3	60	11.0
	4	45	−2.00

Nonbonded Interactions
$U_{nb} = 4\varepsilon_{ij}\left[\left(\frac{\sigma_{ij}}{r_{ij}}\right)^{12}-\left(\frac{\sigma_{ij}}{r_{ij}}\right)^{6}\right]+\frac{q_iq_j}{4\pi\varepsilon_0}\left(\frac{1}{r_{ij}}+\frac{\varepsilon_{rf}-1}{2\varepsilon_{rf}+1}\frac{r_{ij}^2}{r_c^3}\right)$

atom	σ (nm)	ε (kJ mol^{-1})	q (e)
H_c	0.0	0.0	0.128
O	0.3066	0.81	−0.256
C_c	0.340	0.30	0.550
O_c	0.296	0.82	−0.410
C_{a1}	0.340	0.30	−0.032
C_a	0.340	0.30	−0.118
H_a	0.272	0.075	0.118
C_b	0.340	0.31	0.050
H_b	0.240	0.080	0.049

[a] C_a, C_b, and C_c represent an aromatic, an aliphatic, and a carbonyl carbon atom, respectively. C_{a1} represents a carbon atom, involved in an aromatic ring, adjacent to a carbonyl carbon atom. Similarly, H_a, H_b, and H_c represent a hydrogen atom connected to an aromatic carbon atom, an aliphatic carbon atom, and an oxygen atom, respectively. O_c represents an oxygen atom connected to C_c with double bonds. When there is no difference between the parameters of C_a and C_{a1}, subscript 1 is dropped. [b] These values are taken from Allinger et al.[45]

Force Field

An all atom model of PET has been developed for better understanding of the structure and dynamics of PET chain. The force-field parameters are mainly taken from Cornell et al.[44] and from Allinger et al.[45] The main modification in the force field is tuning the torsional potentials for rotations around bonds I−VI in Figure 1. As it is founded by Cail et al.,[22] the main torsional potential to be calculated is the rotation around bond V. Experimental spectroscopic measurements[46−52] of the conformer populations of the glycol unit in amorphous PET samples show that the *gauche* conformer populations ranges between 75 and 88%. However, a detailed analysis of the polyoxyethylene chain by Abe et al.[53] showed that the conformer population of glycol unit (bond V) is more complex than can be represented by the statistical weights in the RIS model. A similar phenomenon was observed by Yoon[54] in the simulation of poly(oxyethylene), in which lower *gauche*$^{(\pm)}$ *gauche*$^{(\mp)}$ conformations of the glycol unit were found in the melt. The favorability of such conformations is attributed to the intermolecular O···CH interactions.[54] Therefore, in this work, the potential energy barrier for torsions were found by performing a series of MD simulations of PET to achieve a correct conformer population of bond V, to get a correct value of characteristic ratio, and to predict experimentally determined dipolar ratios. Another modification in the force field is the slight change in the Lennard-Jones potential parameters to match the calculated densities, over a wide range of temperatures and pressures, to the experimental values.[12,27,28] The force-field parameters are reported in Table 1. The calculation results are described in the following sections.

Simulation Details

Having prepared a single hydroxyl-terminated PET chain consisting of 120 repeat units with a total number of 2643 atoms (molecular weight ∼23000 g mol^{-1}), according to the procedure outlined above, MD simulations were carried out using our simulation package, YASP.[55,56] All nonbonded interactions were truncated at 0.95 nm with a reaction field correction for the Coulombic interactions.[57] The effective dielectric constant was taken equal to the experimental value, 3.6.[58] An atomic Verlet neighbor list was used, which was updated every 15 time steps, and the neighbors were included if they were closer than 1.0 nm. All bond lengths were constrained using the SHAKE iterative procedure,[59,60] with a relative tolerance of 10^{-6}. The leapfrog variant of the velocity Verlet algorithm[57] was employed to integrate Newtonian equations of motion, with a time step of 1.5 fs. The system was coupled to heat baths at a fixed temperature and a fixed pressure according to the method of Berendsen et al.[61] The temperature and pressure coupling times were 0.2 and 5.0 ps, respectively. At the very beginning, a chain of PET generated using the RIS model,[22] as described above, was immersed into a simulation box of rather big size, about 40 nm, in order to avoid possible close contacts of nonbonded atoms. The box was then allowed to relax under the fixed imposed external pressure (0.1 MPa) and at a rather high initial temperature (600 K) for sufficiently long time. The simulations were performed for 15.0 ns for relaxation and up to 30.0 ns for data collections

Results

Characteristic, Dipolar, and Ethylene Glycol *Trans*/*Gauche* Ratios. We have fitted the torsional angle barriers against the experimental results for characteristic ratio,[42] dipolar ratio,[12] and ethylene glycol *trans*/*gauche* ratio.[46−52] To do this, the bond lengths, bond angles, and dihedral angles as well as their corresponding energy barriers were kept fixed,

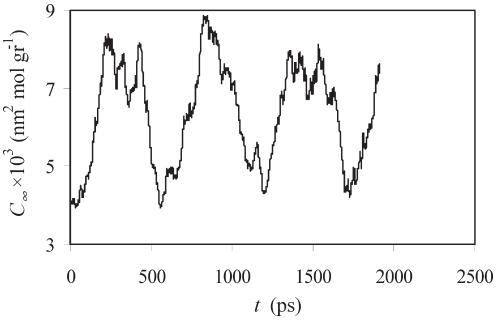

Figure 2. Time evolution of the characteristic ratio of PET 120-mer. The average value is 6.3×10^{-3} nm^2 mol g^{-1}.

according to the values reported in Table 1, and the torsional states were adjusted as follow.

It is known that the bulk polymer obeys the so-called Θ conditions, which are characterized by unperturbed dimensions. Therefore, the experimentally estimated characteristic ratios could be achievable from the results of MD simulations. To this end we have put the polymer chain in a large cubic box (box length 40.0 nm), to avoid the effects of periodic boundary conditions, and excluded the long-range nonbonded and Coulombic interactions. Similar to the previously reported conclusions,[21,22,25,26,43] we also found that the characteristic ratio is sensitive to *trans*/*gauche* ratio around bond V. Moreover, experimental findings, as addressed above, show that *trans* fraction for bond V conformer ranges between 0.12 and 0.25, depending on the thermal history of the material and the experimental method used.[46−52] Therefore, we have also performed MD simulations of bulk PET and tried to fit the torsional barrier of bond V. Another experimentally determined parameter, used as a target parameter to adjust torsional states of PET is dipolar ratio, D_∞, defined as

$$D_\infty = \frac{\langle \mu^2 \rangle}{N_D \langle \mu_D^2 \rangle} \tag{2}$$

where $\langle \mu^2 \rangle$ is the mean-square dipole moment of the unperturbed polymer, N_D is the number of dipoles (monomers), and μ_D is the monomer dipole moment. The dielectric measurements by Coburn and Boyd[12] show that the dipolar ratio in the bulk polymer ranges between 0.28 and 0.32 over a small temperature range of 353−373 K. In adjusting the torsional states of PET, we got similar conclusions as Hedenqvist et al.,[25] in that the characteristic ratio is more sensitive to the bond V *trans*/*gauche* ratio and the dipolar ratio is more sensitive to the possible conformations around bonds II, IV, and VI. But the results of Hedenqvist et al.,[25] show that dipolar ratio is quite insensitive to the to the bond V *trans*/*gauche* ratio, while our results show a considerable *trans*/*gauche* dependency of dipolar ratio. As stated earlier polymer adopts equal populations of *cis* and *trans* conformations with respect to bond II. Therefore, torsional energy barriers for bonds IV/VI were fit to achieve correct dipolar ratios.

We performed MD simulation of bulk PET and PET chains in vacuum, as explained above, to adjust the torsional energy barriers against the target values of characteristic, dipolar, and ethylene glycol t*rans*/*gauche* ratios. Meanwhile the nonbonded parameters of the force field were taken care of in order to achieve a good representation of pressure-volume-temperature of bulk PET, as it is described in the following section. The final results are tabulated in Table 1. Employing this force field for a 120-mer sample of PET in

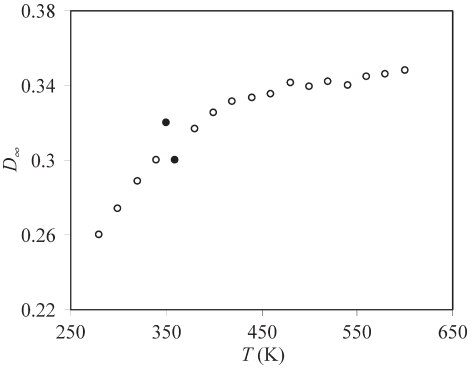

Figure 3. The calculated dipolar ratio of PET as a function of temperature. Open markers represent our calculations and the filled markers represent experimental data.[12]

vacuum at 353 K, a temperature at which the experimental data[14] are reported, show that the characteristic ratio is fluctuating around 6.3×10^{-3} nm^2 mol g^{-1}, which is quite consistent with the findings of Gilmer et al.,[42] and with the calculations by Taylor et al.,[21] by Cail et al.,[22] and by Sasanuma.[43] The results are shown in Figure 2. In previous simulations by Hedenqvist et al.,[25] Boyd and Boyd,[26] and Karayiannis et al.,[32] a characteristic ratio around 10×10^{-3} nm^2 mol g^{-1} has been reported, which is quite a bit larger than the experimental findings[42] and recent theoretical calculations.[21,22,43]

The results of our MD simulations in the bulk show that our calculated dipolar ratio at 353 K locates close to the reported bulk value by Coburn and Boyd.[12] Similar calculations are performed over the temperature range 280 K-600 K and the results are compared with the experimental reports of Coburn and Boyd[12] in Figure 3. Our results show a smaller temperature dependency of the dipolar ratio as the reported values by Hedenqvist et al.[25]

We have also calculated *trans* fractions for bonds I−VI conformers over a wide temperature range. The results are shown in Table 2 and are compared with the calculated values by Hedenqvist et al.,[25] by Boyd and Boyd,[26] and by Sasanuma[43] and with the experimental measurements.[46−52] As it is clear from the results in Table 2, our calculated values locate within the range of experimental measurements, as addressed in the text. In the original work by Hedenqvist et al.,[25] no attention was paid to the population of ethylene glycol bond conformer, while in their subsequent work, Boyd and Boyd[24] reparametrized torsional parameters of bond V to reproduce experimental results.[46−52] Our results, tabulated in Table 2 are in agreement with the calculations by Boyd and Boyd,[26] and by Sasanuma.[43] Though no direct report is made by Karayiannis et al.[32] on bond V *trans*/*gauche* population ratio, their distribution curves shows a substantial deviation of this ratio compared to experiment.[46−52] The distribution functions for different torsional states of PET at low and high temperatures are also shown in Figure 4. Here the trans conformation corresponds to 180°. From the results in Figure 4, it is clear that mainly the torsional states around bonds IV, V, and VI play important roles in the structure of polymer.

Pressure−Volume−Temperature Properties. The nonbonded parameters of the force field were adjusted against the density of PET. As described in the preceding section, we started simulating a parent chain of PET at 600 K. Cooling down the relaxed configurations at each temperature with a rate of 5 K ns^{-1}, we generated lower temperature configurations. Following an equilibration cycle of 10.0 ns for higher

Table 2. *Trans* Fractions of Different Bond Conformers as a Function of Temperature[a]

	bond					
			IV, VI		V	
temperature (K)	I, III	II	this work	previous calculations	this work	previous calculations
280	1.0	0.510	0.650	0.49[b]	0.155	0.05[b]
320	1.0	0.500	0.646	0.160	0.152[d]	
360	1.0	0.495	0.641	0.162		
400	1.0	0.498	0.642	0.77[c]	0.170	0.44,[c] 0.152[d]
440	1.0	0.502	0.635	0.179		
480	1.0	0.500	0.629	0.187		
520	1.0	0.499	0.621	0.192	0.159[d]	
560	1.0	0.500	0.615	0.43,[b] 0.72[c]	0.195	0.13,[b] 0.46[c]
600	1.0	0.500	0.610	0.71[c]	0.210	0.46[c]

[a] The numbers identified by superscripts b, c, and d represent the calculated values by Sasanuma,[43] by Hedenqvist et al.,[25] and by Boyd and Boyd,[26] respectively. These values may not exactly be reported at the same temperature, but at a close temperature to what indicated here. The calculated values for *trans* fractions of bond conformers I, II, and III by these authors are almost identical to the results reported in columns 1 and 2; therefore, we skip comparing our results with theirs in this table. The experimental values[46−52] on *trans* fraction of bond V ranges between 0.12 and 0.25. [b] Sasanuma.[43] [c] Hedenqvist et al.[25] [d] Boyd and Boyd.[26]

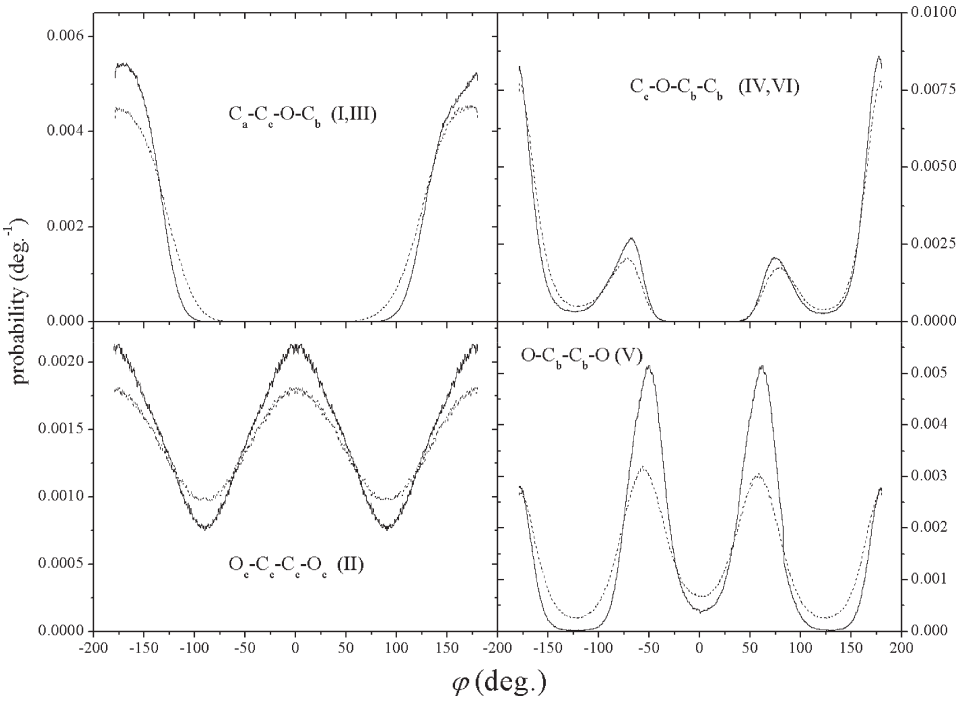

Figure 4. Distribution of torsional angles in PET. The torsions as well as the bond types are shown in the figure. The solid and dashed curves represent the results at 280 and 600 K, respectively.

temperature ($T \geq 400$ K) configurations, a production run of 30.0 ns was performed and trajectories were recorded every 0.75 ps. For lower temperature configurations ($T < 400$ K) the equilibration step was extended to 15.0 ns. The results of the calculated density of PET over a wide range of temperatures and pressures are shown in Figure 5 and are compared with the previous simulation results by Hedenqvist et al.,[25] by Boyd and Boyd,[26] and with the experimental data.[12,27,28] The agreement of the calculated densities of the 0.1 MPa isobar with experiment is remarkable.[12,27,28] At the higher-pressure isobar (192 MPa), no experimental density of the glassy PET exists for comparison. Here the results can only be compared against a few experimental data point of PET melt.[27] The breaks at each isobar (342 K at 0.1 MPa isobar and 395 K at 192 MPa isobar) indicate the glass transition temperatures of PET, which are in close agreement with experiment (343 K, and 393 K, respectively).[27] This indicates that the glass transition temperature of PET at ordinary pressures as well as its pressure-dependence nicely agrees with experimental results.

The maximum deviation between our calculated results, reported in Figure 5, and experimental densities is around 0.5%. A comparison of our calculated densities of PET in Figure 5 with previously calculated ones show that MD simulation results by Hedenqvist et al.[25] and by Boyd and Boyd[26] show a considerable deviation from experimental results.[12,27,28] Moreover, the temperature dependency of their results deviates substantially from experimental data,[12,27,28] and hence, their predictions show a glass transition temperature of around 460 and 405 K (at 0.1 MPa), respectively, which is quite higher than experiment.[27] In order to check the pressure dependency of the density of the PET melt at constant temperature, simulations were performed at two isotherms, 567.5 and 615.5 K, over a wide range of pressures ranging from atmospheric pressures to pressures around 200 MPa. Shown in Figure 6 are the calculated density versus pressure for PET compared with experiment.[27] Here the maximum deviation in calculated densities compared to experimental values is around 0.4%. The results in Figure 6 show that our simulation produces accurate compressibilities for PET melt.

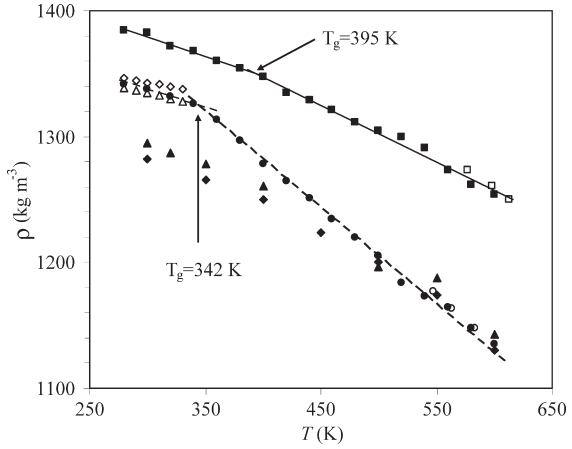

Figure 5. Comparison of calculated results on the density of PET with experiment[12,27,28] and with the results of previous MD simulations.[25,26] The markers (● and ■) represent our calculations at 0.1 and 192 MPa, respectively; the corresponding open markers, the experimental melt data;[27] (△ and ◊) experimental glass data by Coburn and Boyd[12] and by Reddish,[28] respectively; (♦ and ▲), calculated values by Hedenqvist et al.[25] and by Boyd and Boyd,[26] respectively. The solid and dashed lines are the best fits through the calculated densities and the breaks represent the glass transition temperatures. The error bars of our calculated densities locate within the size of markers.

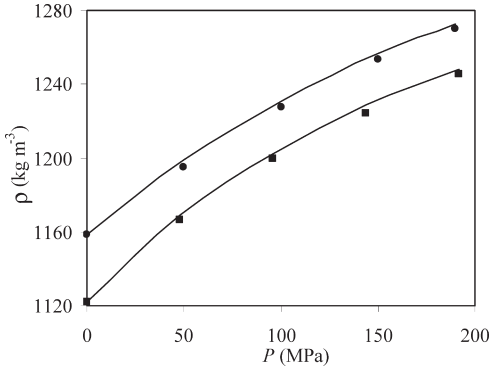

Figure 6. Comparison of the pressure-dependence of the calculated densities of PET with experiment.[27] The solid curves represent our calculations and the markers are the experimental data at 567.5 K (●) and 615.5 K (■).

Structural Characteristics

Total Radial Distribution Function and Structure Factor. Structural information about PET can be obtained at the atomic level by the total (all atom) radial distribution function (RDF), $g(r)$, defined as

$$g(r) = \frac{1}{4\pi r^2 \Delta r} \left\langle \sum_{i=1}^{N} \sum_{j>i}^{N} \delta\left(r - \frac{\Delta r}{2}, r_{ij}, r + \frac{\Delta r}{2}\right) \right\rangle \qquad (3)$$

where r_{ij} is the distance between particles i and j, Δr is the radial interval, δ indicates the Dirac delta function, and brackets indicate the time average. The total RDFs of PET calculated at 300 and 600 K are shown in Figure 7. Peaks belonging to distances below 0.2 nm, which are due to atoms separated with each other by one and/or two bonds, are not shown in the figure, for the sake of clarity. The peaks at around 0.22, 0.24 nm, and 0.27 nm correspond to the distance between aromatic carbon atoms with carbonyl oxygen atoms, $C_a-C_c-O_c$ (0.22 nm) and the distance between carbon atoms in phenylene rings, $C_a-C_a-C_a$ (0.24 nm), and $C_a-C_a-C_a-C_a$ (0.27 nm). Peak at around

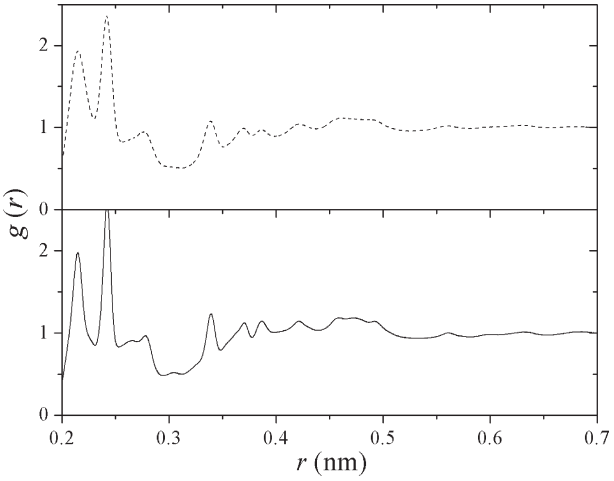

Figure 7. Calculated total radial distribution function of PET at 300 (solid curve) and 600 K (dashed curve).

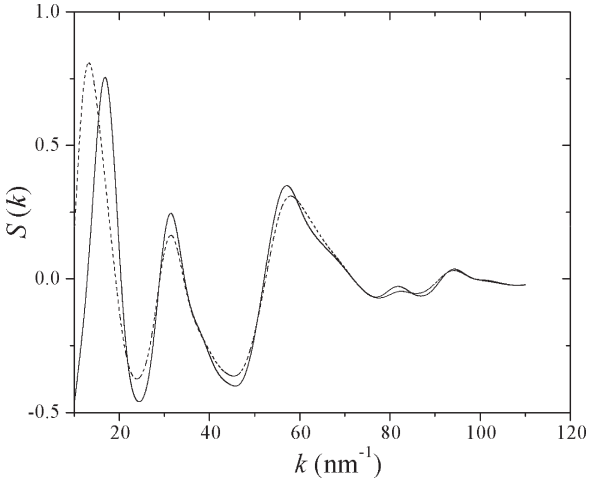

Figure 8. Calculated structure factor of PET at 300 (solid curve) and 600 K (dashed curve).

0.34 nm corresponds to the distance between oxygen atoms in ethylene glycol *gauche* conformers ($O-C_b-C_b-O$). All other peaks up to 0.45 nm reveal clear intramolecular features. The wide peak at around 0.47 nm shows both intramolecular and intermolecular characteristics. Increasing the temperature makes the peaks wider and removes some small characteristics from the wide peak at 0.47 nm. The peaks at longer distances are due to intermolecular distances. By Fourier transforming the radial distribution function, one can obtain the static structure factor as:

$$S(k) = 4\pi\rho \int_0^\infty [g(r) - 1] \frac{\sin(kr)}{kr} r^2 \, dr \qquad (4)$$

The structure factor, $S(k)$, can be compared with experimental X-ray diffraction results.[62] The results for the static structure factors of PET at 300 and 600 K are shown in Figure 8. The calculated $S(k)$ completely follows the experimental curve,[62] in that the three peaks with maximum intensities at 15, 30, and 55 nm^{-1} are seen at the same distances in the experimental intensity versus k values.[62] Comparison of calculated $S(k)$ curves at 300 and 600 K shows that the first peak, at around 15 nm^{-1} (which is equivalent to the RDF peak at 0.42 nm) shifts to higher distances at higher temperatures. The rest of the peaks, corresponding to intramolecular distances, are left almost

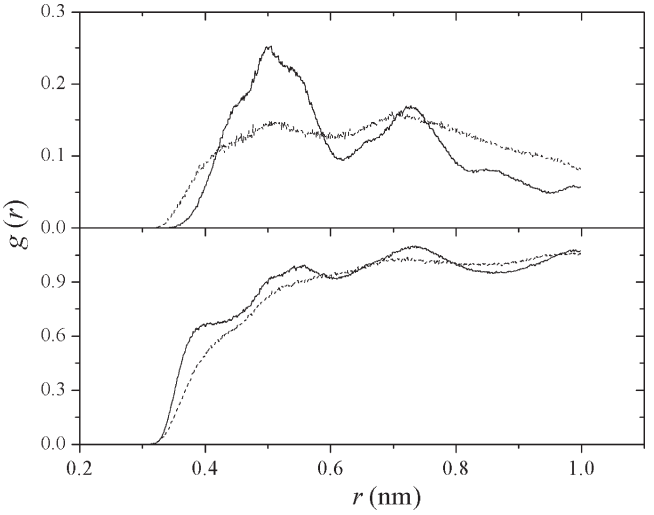

Figure 9. Top panel: Center-of-mass radial distribution function for directly connected phenylene groups of PET at 280 K (solid curve) and 600 K (dashed curve). Bottom panel: The same as top panel, but for all phenylene groups.

unchanged. This shows that the first peak of $S(k)$ has an intermolecular origin, a conclusion which is confirmed by X-ray diffraction experiment.[62]

Orientation Distribution Function. It is instructive to analyze the immediate surroundings of phenylene groups in PET, by looking at their distributions and their mutual orientations. Shown in Figure 9 are the center-of-mass RDFs of all phenylene rings of PET at 280 and 600 K. The RDF at 280 K shows more structure, with the first peak locating at around 0.35 nm. To elucidate the origin of this peak, the center-of-mass RDF for directly connected phenylene rings in the backbone (phenylene groups next to each other), at 280 and 600 K, are also shown in Figure 9. A comparison of both RDFs show that the first peak at around 0.35 nm has the interchain characteristics, as the two consecutive phenylene groups in PET, which are tied together by the polymer backbone are forced to stay at longer distances (peaks at 0.5 and 0.7 nm in the top panel of Figure 9). The RDF for all phenylene rings at 280 K shows two more peaks at 0.52 nm and 0.65, which are broadened at higher temperatures. At this point it is worth mentioning that recent molecular orbital calculations of Sasanuma and Suzuki[63] on conformational probabilities of ethylene glycol dibenzoate, a model compound for PET, shows a phenylene−phenylene distance higher than 0.75 nm. Integration of our RDF results at 600 K, however, show the existence of 6% of phenylene groups with their center-of-mass separations less than 0.5 nm. Our analysis shows that the existence of such conformations is due to gauche conformers of bond V, in which the torsional angle is around 10°. Such conformations, of course, exist in bulk sample (see Figure 4) as a result of packing effects, however, molecular orbital energy minimization methods on a small molecule such as ethylene glycol dibenzoate do not show the existence of higher-energy *cis* conformation.

It is interesting to look at the orientation of phenylene groups. The orientation of coplanar phenylene groups can be characterized by the ring normal vectors, $\boldsymbol{u}$. This vector is defined as the appropriately normalized arithmetic mean of the normals of the two planes, each defined by three nonconsecutive carbon atoms of the phenylene groups.[64] The mutual orientation of two phenylene rings is described by orientational distribution functions (ODF) in terms of the

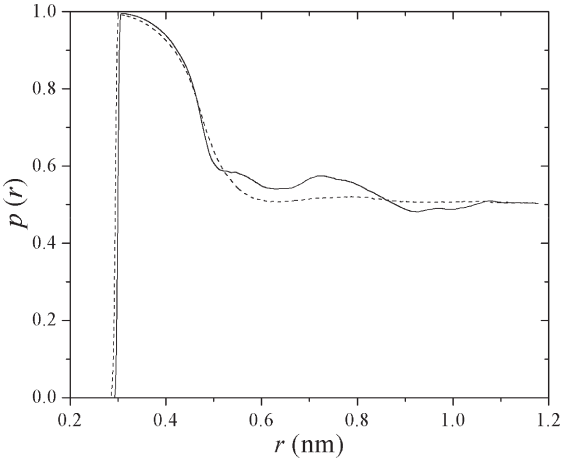

Figure 10. Orientation distribution function for normals of phenylene rings. The solid and dashed curves represent the results at 280 and 600 K, respectively.

first and/or second Legendre polynomials. The first Legendre polynomial is expressed as:

$$p(r) = \langle \mathbf{u}_i \cdot \mathbf{u}_j \rangle \tag{5}$$

where $\boldsymbol{u}_i$ and $\boldsymbol{u}_j$ are the ring normals, and p (r) is the first Legendre polynomial. Since the rotation of phenylene groups by 180° leads to symmetrically equivalent orientations, we use the absolute value of the scalar product $|\boldsymbol{u}_i.\boldsymbol{u}_j|$. The value of p (r) so defined is 1 for two coplanar rings, 0 for a T-shaped arrangement, and $^1/_2$ for a random distribution of orientations.

The ODFs for the phenylene normals as a function of distance between the ring centers are shown in Figure 10. The results in Figure 10 show that, at short distances (∼0.3 nm), phenylene rings are predominantly coplanar. This finding is in contrast with the results reported by Boyd and Boyd,[26] who observed no preferential orientation of phenylene groups. However, the preferential planar orientation of phenylene rings at short distances has also been found[64] in polystyrene and polystyrene-benzene mixtures at almost the same distance as here (∼0.3 nm). The ODF peak quickly decays with increasing distance and little structure is visible beyond 1.0 nm. At low temperatures, the phenylene groups at higher distances show just very small preferential coplanar orientations (see Figures 9 and 10). Increasing the temperature has little effect on the preferential orientation of phenylene groups at short distances (∼0.3 nm), but forces the phenylene groups at higher distances (> 0.5 nm) to adopt a random orientation.

Chain Dynamics

Individual and Collective Dipole Moment Correlation Functions. Particular useful information about the chain dynamics can be obtained by calculating the collective dipole−dipole autocorrelation functions, which can be expressed in terms of the first Legendre polynomial as:

$$\langle p(t) \rangle = \frac{\langle \boldsymbol{\mu}(t).\boldsymbol{\mu}(0) \rangle}{\langle \mu(0)^2 \rangle} \tag{6}$$

where $\boldsymbol{\mu}$ is the dipole moment vector of the PET chain, and p is the first Legendre polynomial. The function is related experimentally to the normalized time-dependent retarded dielectric constant.[26] Here we have calculated the collective dipole moment autocorrelation functions at different temperatures by averaging over long trajectories. The results at different temperatures are shown in Figure 11. The collective

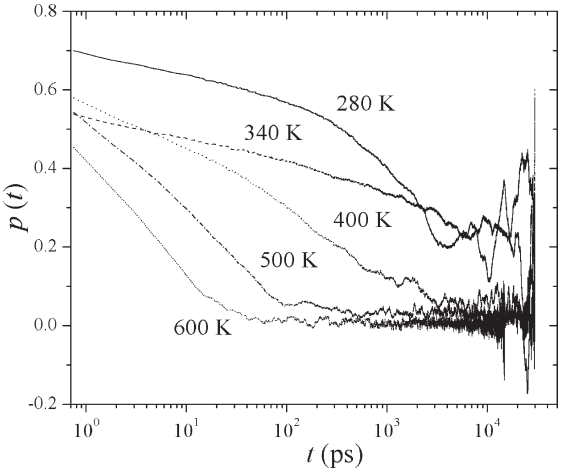

Figure 11. Autocorrelation function for the collective dipole moment vectors.

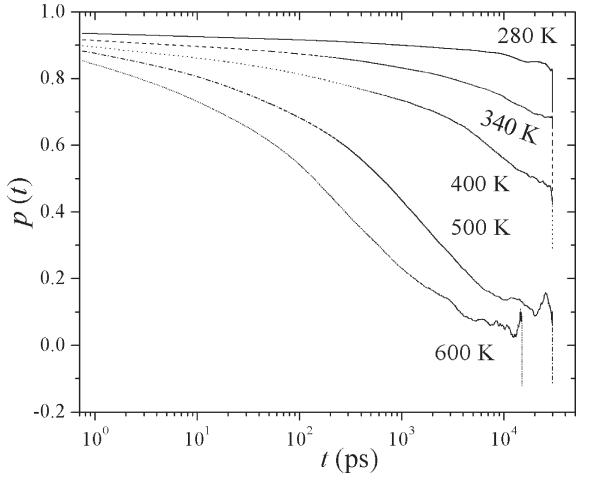

Figure 12. Same as Figure 11 for individual dipole moment vectors.

dipole moment correlation function is quite noisy and decays fast. In contrast the individual dipole moment correlation function, which is defined by a similar expression as eq 6, but the correlating vectors are the dipole moment vectors of individual monomers, decays much slower and is less scattered. In Figure 12, we have shown similar correlation functions for the individual dipole correlation functions. The results in Figures 11 and 12 show that the chain dynamics is much faster at higher temperatures. In the glassy state (the curves at 280 and 340 K) the decay rate is very slow, due to the slower dynamics of chains. Fitting the relaxation curves in Figures 11 and 12, with the so-called Kohlraush−Williams−Watts (KWW) stretched exponential function,[65] one can obtain the relaxation times, τ, for collective and individual dipole correlations. Shown in Figure 13 are the Arrhenius plots of $\log(\tau)$ vs $1/T$ for collective and individual dipole relaxation times. The calculated activation energy for the collective dipole relaxation, 49.8 kJ mol^{-1}, is close to the β-mobility activation energy reported by Bartos et al.,[66] 57.4 kJ mol^{-1}, but the slope for individual dipole relaxation (27.2 kJ mol^{-1}) deviates substantially from this value. Here we got the same result as Boyd and Boyd,[26] who observed that the collective dipole relaxation, which is directly related to the experiment gives a closer activation energy to the experiment. It is worth mentioning that β-relaxation in PET consists of two different relaxation processes. The higher temperature process is due to the motion of phenylene

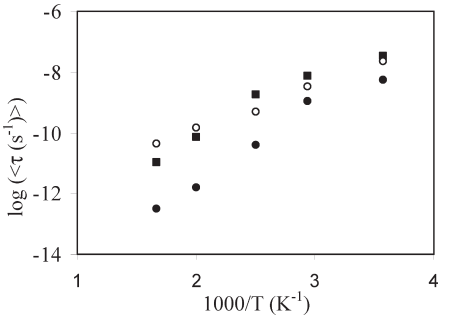

Figure 13. Temperature-dependence of relaxation times for (●) total dipole moment, (○) individual dipole moment, and (■) phenylene group autocorrelation functions.

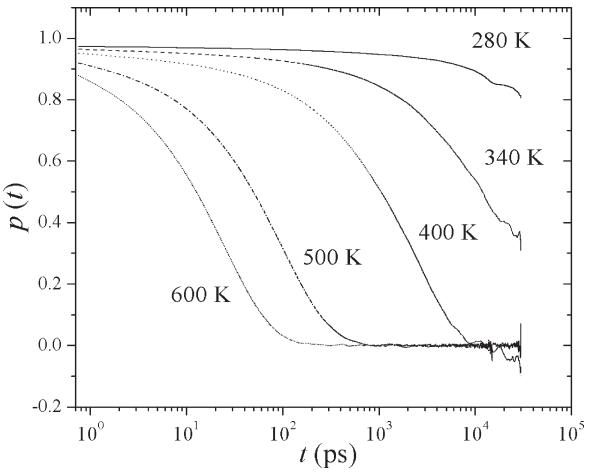

Figure 14. Same as Figure 11 for vectors normal to the phenylene groups.

groups, whereas the lower temperature process is due to the motion of carbonyl groups.[66] McGonigle et al.[67] argued that within the temperature range 200−240 K, the only relaxing entity is the carbonyl group. At higher temperatures the phenylene groups become mobile. Dynamic mechanical and dielectric analysis results of Maxwell et al.[68] attributed activation energies of 57 and 70 kJ mol^{-1} to the lower temperature and higher temperature processes, respectively. As it is claimed by Boyd and Boyd,[26] β-relaxation is complex in that it appears to consist, at much lower temperatures and hence with the possibility of higher resolution than is accessible to MD simulation, of overlapping components. However, the MD calculated activation energy for collective dipole relaxation, as it is also shown by Boyd and Boyd,[26] corresponds to the motion of carbonyl groups.

Orientational Correlation Function for Phenylene Rings. The orientational autocorrelation function of phenylene plane normals is a measure of local mobility in PET. The orientational autocorrelation function is defined analogous to eq 6, where the plane normals replace the dipole vectors, as defined above. The calculated phenylene autocorrelation functions are given in Figure 14. From the results it is clear that the reorienting vectors decorrelate much faster at higher temperature, due to faster rotation/movement of phenylene groups. Similar information can be obtained by analyzing the rotational dynamics of carbonyl groups, as the O_c-C_c-O group is in the same plane as phenylene rings. Our calculations show that reorientational correlation functions for CO bond vectors are quite similar to phenylene normal correlation functions. The same conclusion has already been reported by Karayiannis et al.[32]

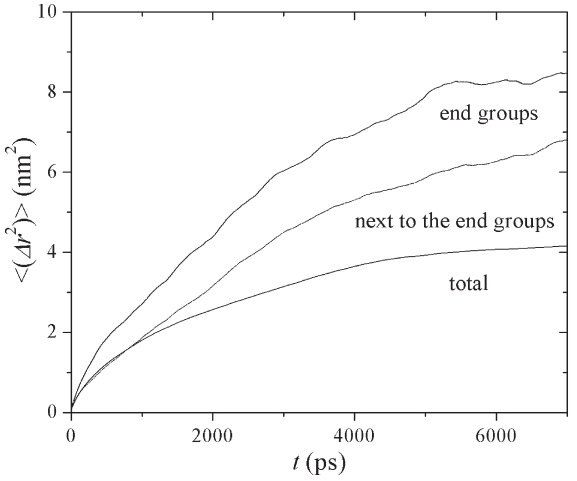

Figure 15. Mean-square-displacements for: carbon atoms of all phenylene groups in the backbone, carbon atoms of the phenylene end groups, and carbon atoms of the next to the end phenylene groups.

Here also the relaxation curves are fitted with KWW function, and the results are shown in Figure 13. The calculated activation energy, 47.5 kJ mol^{-1}, is again close to the β-mobility activation energy reported by Bartos et al.,[66] 57.4 kJ mol^{-1}. The close activation energies of phenylene and collective dipole correlation functions is due to the correlative motions of the adjacent phenylene and carbonyl groups in PET. The same conclusion is reported by Boyd and Boyd.[26]

Local Translational Mobility. The mean-square displacement (MSD), defined

$$\langle(\Delta r)^2\rangle = \langle(\mathbf{r}_i(t) - \mathbf{r}_i(0))^2\rangle \quad (7)$$

is a convenient measure of atom mobility. Here $\boldsymbol{r}_i$ is the position vector of the i_{th} atom. The shape of MSD curve depends on the underlying physical process; it is an increasing function of time for a diffusive atom, while it reaches a constant value with the passage of time for a stationary atom. Here, the MSD curves are calculated in three cases: (1) for all carbon atoms of phenylene groups in the backbone, (2) for carbon atoms of the phenylene end groups, and (3) for carbon atoms of the next to the end phenylene groups. The averaging is performed over all atoms and over all time origins. The results at 600 K are shown in Figure 15. Our results show that at high temperatures the mobility of backbone is quite different from that of phenylene end groups. In fact, the phenylene end groups are much mobile than the corresponding groups in the polymer backbone. Translational displacement of the backbone, however, occurs very slowly, because for backbone to have a noticeable displacement, big distortions along the backbone are required. On the other hand, the end groups do not need such big perturbations. Comparison of the results for phenylene end groups and for next to the end phenylene groups shows that increasing the distance from chain ends, leads to a considerable decrease in translational mobility.

Cage Effect. The shape of the mean-square fluctuation curve illustrates whether there exists a normal or an anomalous diffusive motion of atoms. At higher temperature a diffusive motion is observed, while at lower temperatures the bent shape of the curves, indicate clearly that diffusion is anomalous on this time scale, i.e., that atoms are not free to perform random motion.

In Figure 16 we have shown in more detail the MSD for the carbon atoms of phenylene groups in the backbone at different temperatures. Similar to the treatment of Lyulin and Michels,[69] to remove the temperature dependency of the MSD, all curves are multiplied by a factor T_0/T, where T_0 = 600 K. The results in Figures 16 show that at very short times ($<$ 1 ps) the slope of MSD curve for phenylene groups in the backbone is between 1 and 2 (a slope of 2, shown in the Figure 16, would be the case for pure ballistic regime). At longer times and at temperatures higher than the glass transition temperature, the slope changes to 0.65, close to the prediction of Rouse model (slope = 0.5), and very close to the MD simulation results of Lyulin and Michels[69] on long-chain polystyrene. The crossover between these two regimes of diffusion is known as the cage effect.[69] In other words, the surrounding monomers form a cage, in which polymer can do restricted motions. The difference in the slopes obtained here and the prediction of Rouse model can be attributed to shortness of chain length. Moreover, in this atomistic simulation we do not have enough statistics to distinguish the Rouse mode. Decreasing the temperature, to the glassy regime, the afore-cited two regions (regions with slope close to 2 and 0.5, respectively), are separated by a plateau. At 280 K, the plateau probably extends over the whole time accessible in our simulation and beyond. As explained before, the cage effect is responsible for the crossover observed in Figure 16.

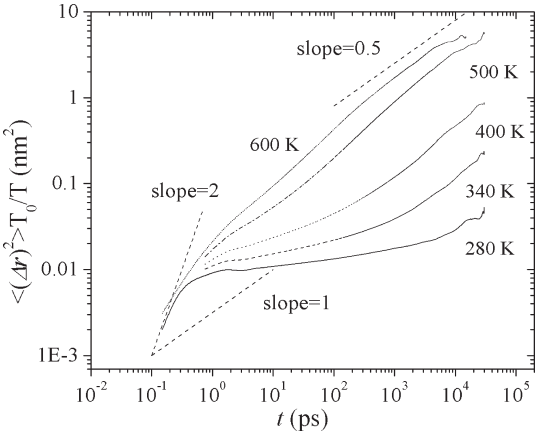

Figure 16. Mean-square-displacement of phenylene groups along PET backbone. Dashed lines with slopes of 0.5, 1, and 2 are drawn to make the comparison of the slopes easier.

Summary

An accurate force field has been developed and employed to perform MD simulation of a long-chain PET. The torsional barrier parameters of the force field were calculated by targeting the experimental characteristic ratio,[42] the dipolar ratio,[12] and the ethylene glycol *gauche*/*trans* ratio.[46−52] Good agreement between the calculated results and the experimental findings, as well as the previous reports in the literature, on the characteristic ratio, the dipolar ratio, and the ethylene glycol *gauche*/*trans* ratio is achieved. Our simulation nicely reproduces the experimental pressure−volume−temperature data[12,27,28] over a wide range of temperatures and pressures. The structure of the chain has been confirmed by comparing the calculated structure factor with X-ray diffraction results.[62] It is concluded that the phenylene groups at short distances (around 0.3 nm) adopt a coplanar orientation, while phenylene groups separated with each other by around 0.5 nm, or more, adopt random orientations. Increasing the temperature has no effect on the orientation of short-distant phenylene groups, but increases the random orientation of longer-distant phenylene groups. The calculated relaxation times

for collective dipole moment autocorrelation and reorientation of phenylene groups show activation energies close to the experimental β-motion in PET.[66] Local translational mobilities of phenylene groups in the backbone and side phenylene groups have been investigated by calculating the mean-square displacements as a function of time. It is concluded that the end groups have much higher mobilities than the polymer backbone, and increasing the distance from the chain ends decreases the mobility dramatically. The long-time asymptotic slope of chain displacement at temperatures higher than the glass transition temperature is around 0.65 in close agreement with Rouse model and the results of previous simulations on long chain polystyrene,[69] while in the glassy state, the monomers are restricted to hindered motions in the cages formed by their surrounding monomers.

Acknowledgment. The support of this work by the Alexander von Humboldt Foundation is gratefully acknowledged.

References and Notes

(1) Mastio, D. *Plastics World* **1997**, *55*, 59.
(2) Gupta, V. B.; Bashir, Z. In *PET fibers, films, and bottles. Handbook of Thermoplastic Polyesters*; Fakirov, S., Ed.; Wiley-VCH: Weinheim, Germany, 2002; Vol. *1*, p 317.
(3) Pegoretti, A.; Penati, A. *Polymer* **2004**, *45*, 7995.
(4) Paci, M.; La Mantia, F. P. *Polym. Degrad. Stab.* **1998**, *61*, 417.
(5) Schmidt-Rohr, K.; Hu, W.; Zumbulyadis, N. *Science* **1998**, *280*, 714.
(6) Vigier, G.; Tatibouet, J.; Benatmane, A.; Vassoille, R. *Colloid Polym. Sci.* **1992**, *270*, 1182.
(7) Ezquerra, T. A.; Balta-Calleja, F. J.; Zachmann, H. G. *Polymer* **1994**, *35*, 12.
(8) Bravard, S. P.; Boyd, R. H. *Macromolecules* **2003**, *36*, 741.
(9) Alvarez, C.; Sics, I.; Nogales, A.; Denchev, Z.; Funari, S. S.; Ezquerra, T. A. *Polymer* **2004**, *45*, 3953.
(10) Diego, J. A.; Canadas, J. A.; Mudarra, M.; Belana, J. *Polymer* **1999**, *40*, 5355.
(11) Alves, N. M.; Mano, J. F.; Balaguer, E.; Duenas, J. M. M.; Ribells, J. L. G. *Polymer* **2002**, *43*, 4111.
(12) Coburn, J. C.; Boyd, R. H. *Macromolecules* **1986**, *19*, 2238.
(13) Groeninckx, G.; Reynaers, H.; Berghmans, H.; Smets, G. *J. Polym. Sci., Polym. Phys.* **1980**, *18*, 3111.
(14) Monserrat, S.; Cortes, P. *J. Mater. Sci.* **1995**, *30*, 1790.
(15) Dobbertin, J.; Hensel, A.; Schick, C. *J. Therm. Anal.* **1996**, *47*, 1027.
(16) Jonas, A. M.; Russell, T. P.; Yoon, D. Y. *Colloid Polym. Sci.* **1994**, *272*, 1344.
(17) Santa Cruz, C.; Stribeck, N.; Zachmann, H. G.; Balta-Calleja, F. J. *Macromolecules* **1991**, *24*, 5980.
(18) Ivanov, D. A.; Amalou, Z.; Magonov, S. N. *Macromolecules* **2001**, *34*, 8944.
(19) Tanaka, A.; Sawada, K.; Ishida, Y. *J. Polym. Sci.: Polym. Phys.* **1974**, *12*, 2157.
(20) Auriemma, F.; Corradini, P.; Guerra, G.; Vacatello, M. *Macromol. Theory Simul.* **1995**, *4*, 165.
(21) Taylor, D. J. R.; Stepto, R. F. T.; Bleackley, M.; Ward, I. M. *Phys. Chem. Chem. Phys.* **1999**, *1*, 2065.
(22) Cail, J. I.; Stepto, R. F. T.; Taylor, D. J. R.; Jones, R. A.; Ward, I. M. *Phys. Chem. Chem. Phys.* **2000**, *2*, 4361.
(23) Chen, J.; Zhang, L. *Eur. Polym. J.* **2004**, *40*, 2547.
(24) Kamio, K.; Moorthi, K.; Theodorou, D. N. *Macromolecules* **2007**, *40*, 710.
(25) Hedenqvist, M. S.; Bharadwaj, R.; Boyd, R. H. *Macromolecules* **1998**, *31*, 1556.
(26) Boyd, S. U.; Boyd, R. H. *Macromolecules* **2001**, *34*, 7219.
(27) Zoller, P.; Bolli, P. *J. Macromol. Sci. Phys.* **1980**, *B18*, 555.
(28) Reddish, W. *Trans. Faraday Soc.* **1950**, *46*, 459.
(29) Bharadwaj, R. K.; Boyd, R. H. *Polymer* **1999**, *40*, 4229.
(30) Shanks, R.; Pavel, D. *Mol. Simul.* **2002**, *28*, 939.
(31) Pavel, D.; Shanks, R. *Polymer* **2005**, *46*, 6135.
(32) Karayiannis, N. C.; Mavrantzas, V. G.; Theodorou, D. N. *Macromolecules* **2004**, *37*, 2978.
(33) Hofmann, D.; Fritz, L.; Ulbrich, J.; Schepers, C.; Böhning, M. *Macromol. Theory Simul.* **2000**, *9*, 293.
(34) Hofmann, D.; Heuchel, M.; Yampolskii, Y.; Khotimskii, V.; Shantarovich, V. *Macromolecules* **2002**, *35*, 2129.
(35) Williams, A. D.; Flory, P. J. *J. Polym. Sci., Part A2* **1967**, *5*, 417.
(36) Krigbaum, W. R. *J. Polym. Sci.* **1958**, *28*, 213.
(37) Krigbaum, W. R. *J. Polym. Sci.* **1955**, *18*, 315.
(38) Wallach, M. L. *Makromol. Chem.* **1967**, *103*, 19.
(39) Aharoni, S. M. *Makromol. Chem.* **1978**, *179*, 1867.
(40) Meyerhoff, G.; Shimotsuma, S. *Makromol. Chem.* **1970**, *135*, 195.
(41) Tuzar, Z.; Vosicky, V.; Bohdanecky, M. *Makromol. Chem.* **1979**, *180*, 1399.
(42) Gilmer, J. W.; Wiswe, D.; Zachmann, H. G.; Kugler, J.; Fischer, E. W. *Polymer* **1986**, *27*, 1391.
(43) Sasanuma, Y. *Macromolecules* **2009**, *42*, 2854.
(44) Cornell, W. D.; Cieplak, P.; Bayly, C. I.; Gould, I. R.; Merz, K. M., Jr.; Ferguson, D. M.; Spellmeyer, D. C.; Fox, T.; Caldwell, J. W.; Kollman, P. A. *J. Am. Chem. Soc.* **1995**, *117*, 5179.
(45) Allinger, N. L.; Zhu, Z. Q. S.; Chen, K. *J. Am. Chem. Soc.* **1992**, *114*, 6120.
(46) Heffinger, C. J.; Schmidt, P. G. *J. Appl. Polym. Sci.* **1965**, *9*, 2661.
(47) Cunningham, A.; Ward, I. M.; Willis, A.; Zichy, V. *Polymer* **1974**, *15*, 749.
(48) Yazdanian, M.; Ward, I. M. *Polymer* **1985**, *26*, 1779.
(49) Shen, D.; Long, F.; Wen, Z.; Qian, R. *Makromol. Chem.* **1991**, *192*, 301.
(50) Spiby, P.; O'Neill, M. A.; Duckett, R. A.; Ward, I. M. *Polymer* **1992**, *33*, 4479.
(51) Guévremont, J.; Ajji, A.; Cole, K. C.; Dumoulin, M. M. *Polymer* **1995**, *36*, 2285.
(52) Rodriguez-Cabello, J. C.; Merino, J. C.; Quintanilla, L.; Pastor, J. M. *J. Appl. Polym. Sci.* **1996**, *62*, 1953.
(53) Abe, A.; Furuya, H.; Mitra, M. K.; Hiejima, T. *Comput. Theor. Polym. Sci.* **1998**, *8*, 253.
(54) Smith, G. D.; Yoon, D. Y.; Jaffe, R. L. *Macromolecules* **1993**, *26*, 5213.
(55) Müller-Plathe, F. *Comput. Phys. Commun.* **1993**, *78*, 77.
(56) Tarmyshov, K.; Müller-Plathe, F. *J. Chem. Inf. Mod.* **2005**, *45*, 1943.
(57) Allen, M. P.; Tildesley, D. J. *Computer Simulation of Liquids*; Clarendon Press: Oxford, U.K., 1987.
(58) Kloppers, M. J.; Bellucci, F.; Latanision, R. M.; Brennan, J. E. *J. Appl. Polym. Sci.* **1993**, *48*, 2197.
(59) Ryckaert, J. P.; Ciccotti, G.; Berendsen, H. J. C. *J. Comput. Phys.* **1997**, *23*, 327.
(60) Müller-Plathe, F.; Brown, D. *Comput. Phys. Commun.* **1991**, *64*, 7.
(61) Berendsen, H. J. C.; Postma, J. P. M.; van Gunsteren, W. F.; DiNola, A.; Haak, J. R. *J. Chem. Phys.* **1984**, *81*, 3684.
(62) Gufta, M. R.; Yeh, G. S. Y. *J. Macromol. Sci. Phys.* **1978**, *B15*, 119.
(63) Sasanuma, Y.; Suzuki, N. *Macromolecules* **2009** (on web).
(64) Müller-Plathe, F. *Macromolecules* **1996**, *29*, 4782.
(65) Williams, G.; Watt, D. C. *Trans. Faraday Soc* **1970**, *66*, 80.
(66) Bartos, J.; Hlouskova, Z.; Vulpius, G. *Colloid Polym. Sci.* **1992**, *270*, 229.
(67) McGonigle, E. A.; Daly, G. H.; Jenkins, S. D.; Liggat, J. J.; Pethrick, R. A. *Macromolecules* **2000**, *33*, 480.
(68) Maxwell, A. S.; Monnerie, L.; Ward, I. N. *Polymer* **1998**, *39*, 6851.
(69) Lyulin, A. V.; Michels, M. A. J. *Macromolecules* **2002**, *35*, 1463.